

Article

NO₂ Physical-to-Chemical Adsorption Transition on Janus WSSe Monolayers Realized by Defect Introduction

Lin Ju ^{1,*}, Xiao Tang ², Xiaoxi Li ¹, Bodian Liu ¹, Xiaoya Qiao ¹, Zhi Wang ¹ and Huabing Yin ^{3,*} ¹ School of Physics and Electric Engineering, Anyang Normal University, Anyang 455000, China² College of Science, Institute of Materials Physics and Chemistry, Nanjing Forestry University, Nanjing 210037, China³ Joint Center for Theoretical Physics, Institute for Computational Materials Science, School of Physics and Electronics, Henan University, Kaifeng 475004, China

* Correspondence: julin@aynu.edu.cn (L.J.); yhb@henu.edu.cn (H.Y.)

Abstract: As is well known, NO₂ adsorption plays an important role in gas sensing and treatment because it expands the residence time of compounds to be treated in plasma–catalyst combination. In this work, the adsorption behaviors and mechanism of NO₂ over pristine and Se-vacancy defect-engineered WSSe monolayers have been systematically investigated using density functional theory (DFT). The adsorption energy calculation reveals that introducing Se vacancy could result in a physical-to-chemical adsorption transition for the system. The Se vacancy, the most possible point defect, could work as the optimum adsorption site, and it dramatically raises the transferred-electron quantities at the interface, creating an obviously electronic orbital hybridization between the adsorbate and substrate and greatly improving the chemical activity and sensing sensitivity of the WSSe monolayer. The physical-to-chemical adsorption transition could meet different requirements of gas collection and gas treatment. Our work broadens the application filed of the Janus WSSe as NO₂-gas-sensitive materials. In addition, it is found that both keeping the S-rich synthetic environments and applying compression strain could make the introduction of Se vacancy easier, which provides a promising path for industrial synthesis of Janus WSSe monolayer with Se vacancy.

Keywords: gas sensing; WSSe monolayer; Se vacancy; density functional theory

Citation: Ju, L.; Tang, X.; Li, X.; Liu, B.; Qiao, X.; Wang, Z.; Yin, H. NO₂ Physical-to-Chemical Adsorption Transition on Janus WSSe Monolayers Realized by Defect Introduction. *Molecules* **2023**, *28*, 1644. <https://doi.org/10.3390/molecules28041644>

Academic Editors: Cuiying Jian and Aleksander Czekanski

Received: 31 December 2022

Revised: 20 January 2023

Accepted: 6 February 2023

Published: 8 February 2023



Copyright: © 2023 by the authors. Licensee MDPI, Basel, Switzerland. This article is an open access article distributed under the terms and conditions of the Creative Commons Attribution (CC BY) license (<https://creativecommons.org/licenses/by/4.0/>).

1. Introduction

With the advancement of science and technology, atmospheric pollution is increasingly worsening, thus causing continuous concern. NO_x are major hazardous air pollutants, of which NO₂ is a threat to both the environment and human activities. With respect to human health, NO₂ at concentrations greater than 1 ppm can seriously damages human lung tissue and the respiratory system, triggering or aggravating respiratory diseases, such as emphysema and bronchitis [1,2]. NO₂ is able to generate acid rain, acid fog, and photochemical smog; as ecologically similar to CO₂, it can also cause global warming. In spite of all these drawbacks, NO₂ has some vital industrial applications, e.g., it can be used as a nitric acid component, a rocket propellant [3], a fungicide [4], and a disinfectant [5]. Owing to the above reasons, the detection, collection, and treatment of NO₂ gas are considered to be extremely essential and have received increasingly close attention [6–9]. Numerous absorbent materials have been developed to absorb NO₂, including activated carbon [10], metal–organics [11], metal oxide particles [12–14], etc. For example, bulk phase TiO₂ has been described to be very efficacious as an adsorbent or catalyst in capturing and/or reforming NO₂ [13,14], wherein NO₂ gas molecules can react with metal centers, i.e., Ti⁴⁺ sites, via O, N, or a mixture of both. In the continuous flow reactor, Dalton et al. showed that TiO₂ was effective in converting NO₂ to non-harmful nitrate species under UV radiation [15]. However, the release of NO_x at higher temperatures has been found to be a critical problem when TiO₂ is used in NO_x storage technology [16]. More efforts are

still needed to obtain fundamental insights into the NO₂ adsorption mechanism and to design more sensitive gas sensing devices.

Due to the superior surface-to-volume ratios and massive reaction sites, two-dimensional (2D) materials recently have been receiving attention for gas adsorption, including layered group III–VI semiconductors [17,18], h-BN [19–21], phosphorene [22], transition-metal chalcogenides (TMDs) [23–25], and so on. Lately, a new 2D material, namely Janus 2D TMD material, referring to layers with different surfaces, has generated urgent research interest in energy conversion applications [26–29]. There is a promise that the intrinsic dipole caused by the out-of-plane asymmetric structure in Janus 2D TMD materials tunes the adsorption of molecules on the surface, similar to the situation where an external vertical electric field markedly regulates the gas selectivity and sensitivity of MoS₂ [30]. As a typical Janus 2D TMD material, the Janus WSSe monolayer has been successfully fabricated by implanting Se species into a WS₂ monolayer with pulsed laser ablation plasmas [31] and by heating mixed WS₂ and WSe₂ powders at 1000 °C [32]. Although the adsorption performance on NO₂ gas for WSe₂, the parent material, has been investigated [33], the performance of the Janus WSSe monolayer remains unclear.

In this work, we have explored the adsorption of NO₂ over pristine and Se-vacancy defect-engineered WSSe monolayer with DFT calculations. A systematical discussion of adsorption energy, density of states (DOS), and charge density difference (CDD) is presented to interpret the interaction between the NO₂ gas and the substrate. We found that introducing Se vacancy could cause a physical-to-chemical adsorption transition for NO₂ gas on the Janus WSSe monolayer. Keeping the S-rich environment and applying compression strain are two potential approaches for introducing Se vacancies into the Janus WSSe monolayer. Moreover, for sensing applications, it is also necessary to take into consideration of the desorption behavior of the gas, which could be characterized by the recovery time [34]. Usually, an intense binding suggests that desorption of gas molecules may be challenging, and the device may experience longer recovery times. Based on the Van't Hoff–Arrhenius theory, the recovery time for NO₂ gas adsorption on the pristine and defective Janus WSSe monolayer are investigated, respectively. The purpose of this work is to gain a fundamental understanding of the adsorption of NO₂ gas on the Janus WSSe monolayer and how to design more sensitive gas treatment devices.

2. Results and Discussion

2.1. The Physisorption of NO₂ on Pristine Janus WSSe Monolayer

2.1.1. Screening of Adsorption Sites and Adsorption Energy

The Janus WSSe single layer is formed by the W layer sandwiched between S and Se layers. It has a honeycomb structure similar to the one of its parent materials (WSe₂ and WS₂) [35]. The lattice constant of Janus WSSe is calculated to be 3.26 Å, which sits between the values of its parent materials (WSe₂ and WS₂). Similar to the case of Janus MoSSe [36], the out-of-plane intrinsic dipole, caused by structural asymmetry in the Janus WSSe could be expected to improve the gas sensing properties, which is highly desirable to explore. As shown in Figure 1a,c, in this work, we initially considered the adsorption geometries of NO₂ on both sides of Janus WSSe. For each adsorption case, a gas molecule was placed on the top of a 4 × 4 supercell of the WSSe monolayer, and the whole system was fully relaxed. Furthermore, several possible adsorption sites were considered, including the top site above the center of the hexagon (denoted as **Center**), the top of the W/Se/S atom (denoted as **W/Se/S**), and the top site above the W–Se/(W–S) bond (denoted as **Bond**), with the configurations of the molecule being parallel to the monolayer surface.

According to Equation (1), it could be found that the E_{ads} was dominated by E_{total} because the E_{sub} and E_{gas} were constant at different adsorption sites. Here, the total energy of the gas molecules adsorbed on the Se and S sides of the Janus WSSe at different adsorption sites was calculated to explore the most stable adsorption configuration. As displayed in Figure 1b, for the adsorption of NO₂ on the S-side, we found that the total energy reached a minimum (−396.26 eV) when it was located above the center of the

hexagon (**Center** site), suggesting the most stable adsorption configuration. As to the case of the NO_2 gas molecule adsorbed on the Se-layer, as illustrated in Figure 1d, it was discovered that, when the molecule was located on the top of the W-Se bond (**Bond** site), the system had the lowest total energy (-396.59 eV), which means it was the most stable adsorption site. Moreover, because the total energy of the most stable adsorption configuration on Se-side was 0.33 eV lower than the one on S-side, it could be obtained that the NO_2 gas molecule preferred to adsorb on the Se-side. Hence, for the case of the NO_2 gas molecule adsorbed on the pristine Janus WSSe, we focused on the adsorption configuration, with NO_2 on the **Bond** site at the Se-side. The adsorption energy (E_{ads}) of this adsorption configuration was -0.56 eV, indicating that this adsorption likely belonged to physisorption, where the absolute value of E_{ads} is normally less than 1 eV [34,37–39]. Further exploration of the physisorption is discussed in the following section.

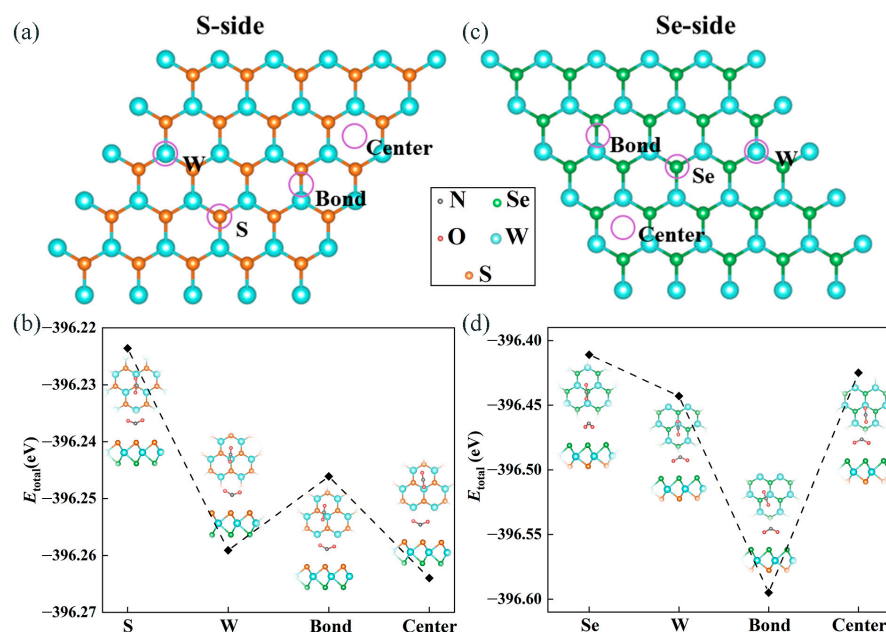


Figure 1. The purple circles indicate the adsorption sites considered in our work at the (a) S and (c) Se side of the pristine Janus WSSe monolayer. The total energy of a NO_2 gas molecule adsorbed on the pristine WSSe monolayer with the four adsorption sites on the (b) S and (d) Se sides, respectively. The illustrations present the top (**upper**) and side (**lower**) views of the optimized configurations of these adsorption systems. The gray, red, orange, green, and blue balls represent N, O, S, Se, and W atoms, respectively.

2.1.2. Adsorption Mechanism

The work mechanism for this physisorption of NO_2 gas molecule adsorbed on pristine WSSe monolayer was meticulously investigated from the aspect of adsorption distance, CDD, Bader charge analysis, and DOS.

As plotted in Figure 2a, after adsorption, the oxygen atoms of the NO_2 gas molecule tended toward the monolayer, and the NO_2 gas molecule remained parallel with the monolayer with a vertical distance of 2.09 Å away from the pristine Janus WSSe monolayer. Moreover, the shortest distances between the O atom from NO_2 molecule and its nearest Se atom was as large as 2.72 Å, greatly beyond the length of Se-O bond (1.81 Å). In addition, as seen in Figure 2b, there were merely 0.21 electrons transferring from the pristine Janus WSSe monolayer to the NO_2 gas molecule, showing the feeble interaction that existed between the substrate and the gas molecule.

The relevant DOS of this adsorption configuration was calculated. As illustrated in Figure 3a–c, both monolayer and gas molecule hardly changed after adsorption in terms of DOS, which was in accordance with the tiny interface transfer electron, suggesting the electronic property of WSSe and NO_2 had no evident changes. There was little orbital

hybridization between WSSe monolayer and NO_2 , which demonstrated that the interaction between the monolayer and molecule was poor, conforming to the discussion above. The orbital hybridization focused mainly on the energy intervals of $-3.76\sim-3.10$ eV and $1.71\sim2.10$ eV, dominantly contributed by the Se p orbital from the WSSe monolayer and the O p orbital from the NO_2 gas molecule (seeing Figure 3d). In addition, the weak orbital hybridization slightly delocalized the DOS peaks of the NO_2 gas molecule, causing its integral area to increase gently. This agreed well with the small amount of gained electron ($0.21 e$) from the WSSe monolayer. According to the above analysis, the adsorption of NO_2 on the pristine WSSe could be confirmed to be physisorption.

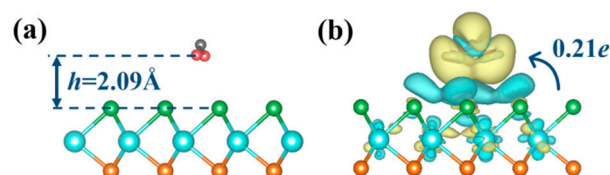


Figure 2. The side view of optimized structure (a) and the charge density difference (b) for the pristine Janus WSSe monolayer with NO_2 gas molecule adsorbed on it. The adsorption distance between the gas molecule and substrate is denoted by h in dark blue. Areas in yellow (cyan) denote charge accumulation (depletion). The isosurface value is set to $0.0003 e \text{ \AA}^{-3}$. The charge transfer between the molecule and the substrate is denoted.

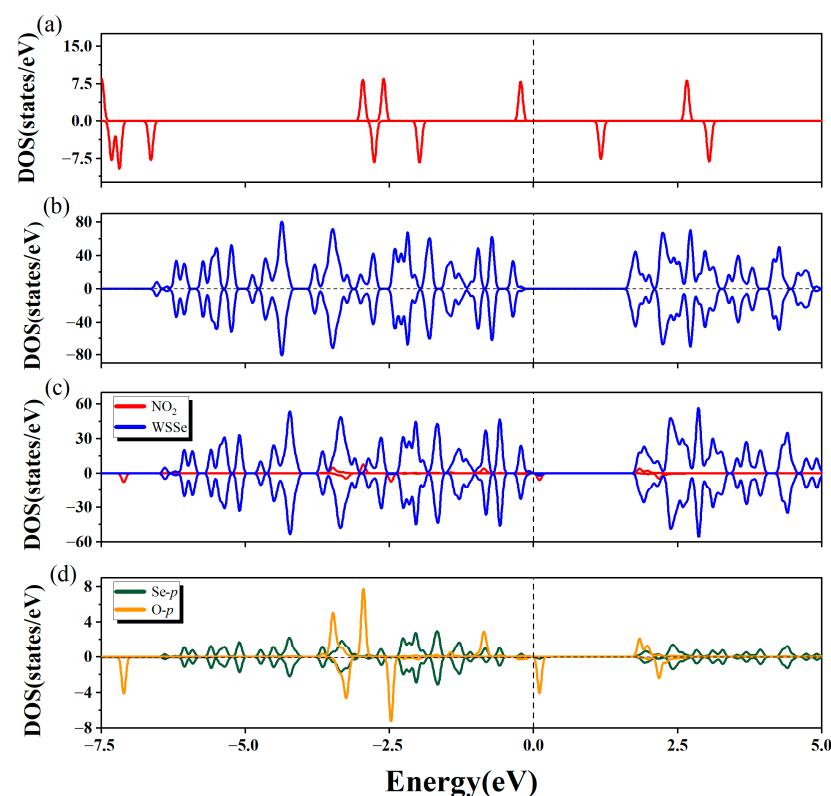


Figure 3. The total density of states of isolated NO_2 gas molecule (a) and clean pristine WSSe monolayer (b). (c) The partial density of states of the adsorption system. WSSe portion is denoted in dark blue, while NO_2 portion is denoted in red. (d) The partial density of states of O p orbitals (denoted in orange) from adsorbed NO_2 gas molecule and Se p orbitals (denoted in green) from the Se atoms in the substrate, which is closest to the gas molecule. The vertical dashed line indicates the Fermi level.

2.2. The Chemisorption of NO₂ on Defective Janus WSSe Monolayer

The adsorption of NO₂ gas molecule on the pristine WSSe is physisorption, which could be utilized as gas collection system. However, for the purpose of treating gas or speeding up chemical reaction, the chemisorption of NO₂ was more essential, which necessitated a more powerful adsorption capacity of the substrate. On the basis of the previously relevant results, introducing some vacancy defects was found to have the ability to influence the electronic property and then improve the stability of some geometric structures effectively [40,41]. Thereby, we introduced vacancy defects in the Janus WSSe monolayer, hoping to obtain an enhanced adsorption capacity of NO₂ gas molecule.

2.2.1. Vacancy Screening

As shown in Supplementary Materials Figure S1, there are two types of vacancy defects in the monolayer WSSe considered, namely sulfur vacancy defect (S vacancy) and selenium vacancy defect (Se vacancy). The formation energies of the defective WSSe monolayer were calculated and are presented in Table 1. It can be seen that the S vacancy had a considerable positive formation energy under both S-rich and Se-rich conditions; the Se vacancy possessed a positive formation energy under the Se-rich condition as well, indicating that the structures of defective WSSe with these vacancies under the corresponding environments were unlikely to form. However, the formation energy of Se vacancy in the S-rich condition was negative, which means that the Se-vacancy could more easily generate Janus WSSe in an S-rich environment. Therefore, in the following calculation, the Se vacancy defect was highly appreciated and was adopted to improve the adsorption capacity of NO₂ on the Janus WSSe monolayer.

Table 1. The formation energy of Se vacancy and S vacancy in the Janus WSSe monolayer under different synthetic conditions.

Vacancy	Synthetic Environment	
	S-Rich	Se-Rich
Se	−0.25 eV	2.78 eV
S	3.35 eV	0.32 eV

2.2.2. Screening of Adsorption Sites and Adsorption Energy

As plotted in Figure 4a, five possible adsorption sites in the defective WSSe monolayer were considered, i.e., the top site above the center of the hexagon (denoted as **Center**), the tops of the W and Se atoms (denoted as **W** and **Se**, respectively), the top site above the W-Se bond (denoted as **Bond**), and the Se vacancy defect (denoted as **Vacancy**). Similar to the case of NO₂ adsorbing on the pristine WSSe monolayer, we employed the total energy of the adsorption system to grasp the most stable adsorption configuration. As displayed in Figure 4b, the total energy attained a minimum when NO₂ adsorbed on the **Vacancy** site, indicating that this site was the most stable location for NO₂ adsorbing on defective WSSe monolayer. In this case, the E_{ads} value was −3.53 eV, which was approximately an order of magnitude more negative than that for NO₂ adsorbing on the pristine WSSe monolayer (seeing Table S1). Apparently, the introduction of Se vacancy would effectively make the NO₂ adsorb more strongly on Janus WSSe. On the basis of the exceptionally negative E_{ads} , we could preliminarily judge that this adsorption behavior belonged to chemisorption, which is further addressed hereinafter.

2.2.3. Adsorption Mechanism

To pursue a more in-depth understanding of NO₂ adsorption on the defective Janus WSSe monolayer, we investigated the adsorption system in terms of the N-O bond length, CDD, electron transfer, and DOS.

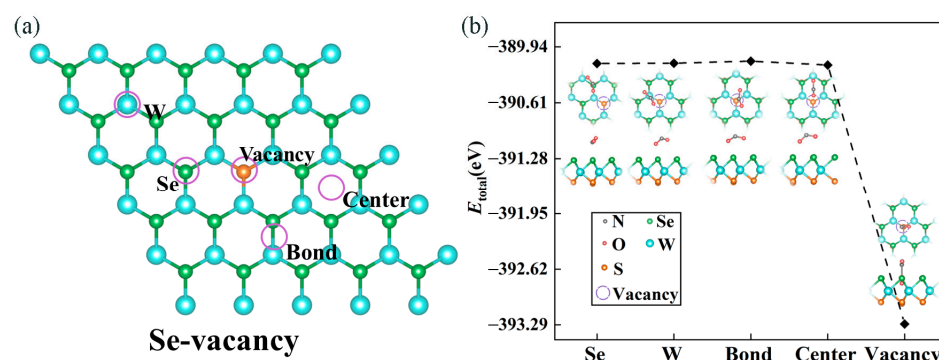


Figure 4. (a) The purple circles indicate the adsorption sites, considered in our work, at the defective Janus WSSe monolayer. (b) The total energy of a NO_2 gas molecule adsorbed defective WSSe monolayer with the five adsorption sites. The illustrations present top (**upper**) and side (**lower**) views of the optimized configurations of these systems. The gray, red, orange, green, and blue balls represent N, O, S, Se, and W atoms, respectively.

As shown in Figure 5a, one of the N-O bonds adopted nearly vertical orientation, with the oxygen atom pointing at the monolayer surface. Additionally, the oxygen atom formed bonds with the three adjoining tungsten atoms at the monolayer surface. Hence, the adsorption behavior definitely was chemisorption, which is in accordance with the result brought by its adsorption energy mentioned above. In addition, in order to quantitatively analyze the behavior changes of gas molecules before and after adsorption, we also measured the length of N-O bonds. Therein, we found that all the N-O bond lengths were 1.20 Å before adsorption, but one of the N-O bond length stretched to 2.55 Å after adsorption (seeing Figure 5b), denoting that the electrons in the gas molecule NO_2 rebuilt after adsorption. As seen in the Figure 5c, there were significant charge redistributions in the adsorption system, and quite a few electrons (1.02 e) migrating from the defective Janus WSSe layer to the adsorbate. Normally, adsorption-induced charge transfer can cause resistivity variation of the system, which is an important index to show the sensing merit and can be measured experimentally for gas sensors [42,43].

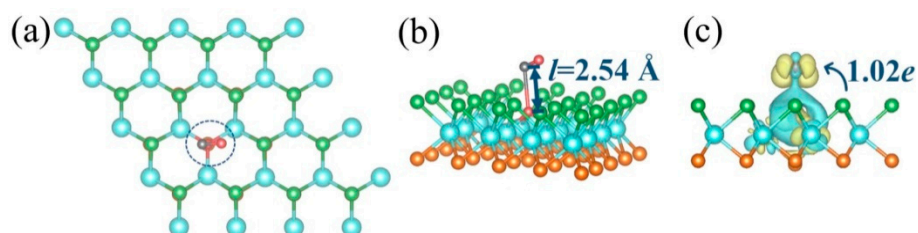


Figure 5. The top (a) and side (b) views of the optimized structures, as well as the CDD (c) of the defective Janus WSSe monolayer with NO_2 gas molecules adsorbed on it. The N-O bond length is denoted by l in dark blue. Areas in yellow (cyan) denote charge accumulation (depletion). The isosurface value is set to 0.002 $e \text{ \AA}^{-3}$. The charge transfer between the molecule and the substrate is denoted.

To gain further insight into the electronic properties of the chemisorption system, we computed the relevant DOS and present them in Figure 6. A significant hybridization existed between the NO_2 gas molecule and the defective Janus WSSe monolayer, which largely concentrated between $-2.5 \text{ eV} \sim -7.5 \text{ eV}$ (seeing Figure 6b). This revealed that there was a strong interaction between them, explaining the phenomenon that NO_2 was tightly attached to the defective WSSe monolayer. Furthermore, as shown in Figure 6c, the interaction was contributed mainly by the hybridization between O p orbital from the NO_2 gas molecule and the W d orbital from the W atoms in the defective WSSe, which bonded to the O atom from the NO_2 gas molecule. By comparing the DOS of NO_2 gas

molecule before and after adsorption (seeing Figures 3a and 6b), it could be discovered that the DOS became delocalized significantly after adsorption, implying that the dramatic redistribution of electrons appeared in the NO_2 gas molecule, which was the reason for the visible N-O bond alteration. Moreover, as shown in Figure 6a,b, the position of the valence band maximum (VBM) of the defective Janus WSSe monolayer moved downward after the NO_2 gas molecule adsorbed on it. The drop in the VBM position corresponded with the Bader charge results, which demonstrated that the defective Janus WSSe monolayer lost $1.02 e$. These outcomes further proved that the adsorption of NO_2 on the defective WSSe monolayer belonged to chemisorption. That is to say, on Janus WSSe, introducing Se vacancy could wonderfully convert the physisorption of NO_2 into chemisorption.

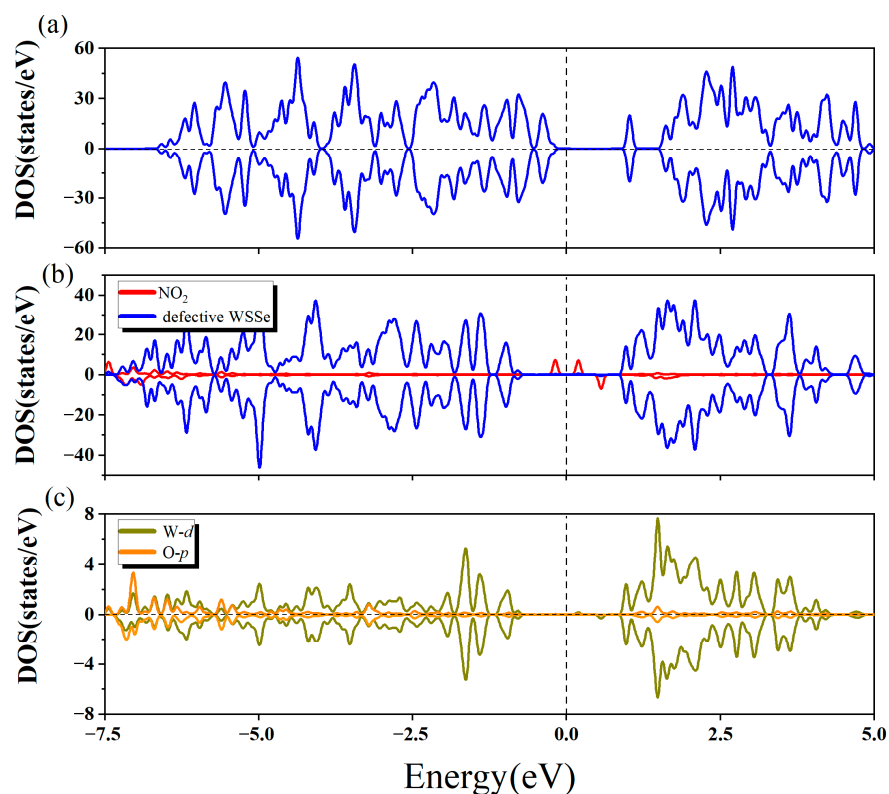


Figure 6. (a) The total density of states of clean defective Janus WSSe monolayer. (b) The partial density of states of the adsorption system. WSSe portion is denoted in dark blue, while NO_2 portion is denoted in red. (c) The partial density of states of O *p* orbitals (denoted in orange) from adsorbed NO_2 gas molecule and W *d* orbitals (denoted in dark yellow) from the three W atoms in the substrate, which bond to the O atom from the gas molecule. The vertical dashed line indicates the Fermi level.

Additionally, though the above calculation results suggest that the defective Janus WSSe monolayer exhibits much improved sensing properties than the pristine one, it is worth noting that the stronger binding may also cause the desorption of the NO_2 gas molecules from the defective Janus WSSe monolayer to be more difficult, and the devices may suffer from longer recovery times. In particular, for the defective Janus WSSe monolayer, the calculated recovery time (10^{46} s) was 10^{50} times that for pristine Janus WSSe monolayer (10^{-4} s) at room-temperature (300 K). Therefore, common methods, for instance, annealing in a vacuum and short UV irradiation [20], likely were not able to regenerate the defective Janus WSSe monolayer to its initial state. However, on the basis of the observation of N-O bond elongation in NO_2 after adsorption, we suppose that NO_2 reduction reaction ($\text{NO}_2 \rightarrow \text{NO}_2^-$) is likely to take place [44], allowing the defective Janus WSSe monolayer to be reversible through water washing, which requires subsequent further investigations.

2.3. Compression Strain Facilitates Vacancy Formation

2.3.1. Strain-Dependent Formation Energy

As is stated above, the S-rich environment is conducive to the formation of Se vacancy in the Janus WSSe monolayer. For a more effective introduction of vacancy in Janus WSSe, some other active methods would still be worth exploring. It is well known that strain can dramatically change the spatial structure and electronic properties of 2D materials [26,45–48]. Therefore, we explored how the strain effected the formation energy of Se vacancy in Janus WSSe, aiming to lower the formation energy with appropriate strain.

As plotted in Figure 7, there was a linear relationship between E_{vac}^* and ε , whether under the uniaxial or the biaxial strains. Furthermore, the greater the compression (smaller the tensile) strains exerted were, the lower the E_{vac}^* became, indicating that the formation energy of Se vacancy decreased linearly as the compression strain rose (tensile strain reduced). That is to say, Se vacancy can be formed more easily under compression strains, which provides a favorable way to generate Se vacancy.

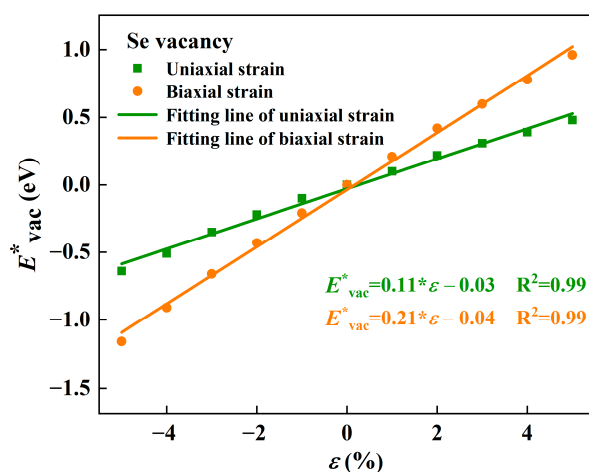


Figure 7. The relative E_{vac}^* of Se vacancy under the different uniaxial (green) and biaxial strains (orange). The value of E_{vac}^* under no strain is selected as a reference value.

In order to give a comprehensive picture of the influence on the formation of vacancy brought by the strain, we also tested the strain effect on S vacancy in the Janus WSSe monolayer. As presented in Figure S2, interestingly, the strain effect on S vacancy was similar to that on Se vacancy, which also had a linear relationship between E_{vac}^* and ε . Specifically, the compression strain induced a drop of the formation energy, while the tensile strain caused the formation energy to increase. Therefore, applying the compression stress can make it easier to form for both S and Se vacancies in the Janus WSSe monolayer. Furthermore, we supposed that it may be an effective method to generate vacancy for other similar structures.

2.3.2. Origin of the Strain-Dependent Vacancy Formation

To analyze the underlying physical mechanism of the strain-dependent behavior of vacancy formation, we calculated the charge difference of the pristine WSSe with and without strain by employing Bader charge analysis. Considering that the influence taken by the -5% – 5% strains were not obvious enough, here, we used 10% strain to enlarge the effect.

We calculated the charge of Se atom under -10% , 0 , and 10% strain, respectively. As shown in Table S2, the valence electron of Se atom was reduced from $6.46 e$ to $6.41 e$ when the exerted strain dropped from 10% to -10% . Compared with the valence electron of Se atom under no strain, the one under -10% strain was closer to $6 e$, which was the valence electron of isolated elemental selenium. This demonstrated that the gain electron of Se atom from W atoms became fewer under -10% strain, and then the interaction between

the Se atom and its surrounding W atoms weakened. Therefore, the Se atom would be more likely to escape from the Janus WSSe monolayer, forming Se vacancy. As to the case of 10% strain, the valence electron of Se atom was greater than the one without strains. This suggested that, the electron transfer increased and the interaction between the Se atom and its adjoining W atoms was enhanced, making the separation of Se atoms from the Janus monolayer more difficult.

2.4. Physical-to-Chemical Adsorption Transition

Based on the discussion above, the pristine Janus WSSe monolayer had a good physical adsorption capability to the NO_2 gas molecule, which could be used to construct gas gathering system. By controlling stoichiometric proportions or applying compression strain, the vacancy, hopefully, could be introduced into the Janus WSSe monolayer. A physical-to-chemical adsorption transition was then caused by the vacancy, as displayed in Figure 8. The defective Janus WSSe monolayer exhibited a well chemisorption to the NO_2 gas molecules, which could be applied to form exhaust gas processor components and gas detectors.

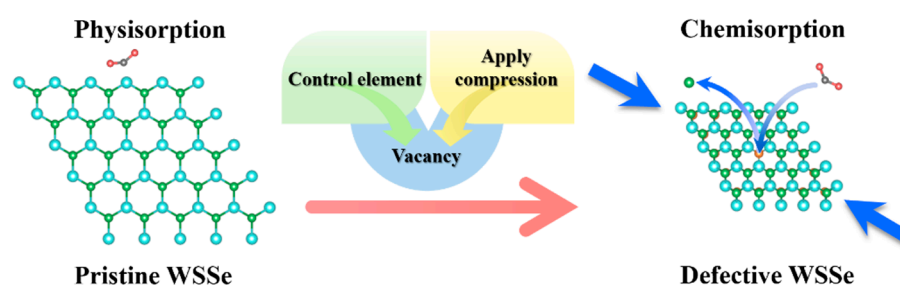


Figure 8. The schematic diagram of NO_2 physical-to-chemical adsorption transition on Janus WSSe monolayer caused by the introduction of Se vacancy. The blue arrows at the opposite corners represent the direction of the imposed compression strain.

3. Conclusions

Owing to the potential environmental threats and commercial value of NO_2 gas, the detection, collection, and handling of NO_2 gas are considered critically necessary. In this work, we performed a theoretical study on the adsorption of NO_2 on the pristine and defective WSSe monolayer. On the pristine WSSe monolayer, according to the tiny adsorption energy, long adsorption distance, and weak electronic orbital hybridization, the adsorption of NO_2 gas molecule is verified to be physisorption. After adsorption, the electronic properties of NO_2 gas molecule and the pristine Janus WSSe monolayer both are essentially the same as those in their isolated states. The introduction of Se vacancy in Janus WSSe monolayer, which could be promisingly realized by S-rich environment or applying compression strain, dramatically raises the transferred-electron quantities at the interface and induces an obviously electronic orbital hybridization between the adsorbate and substrate, causing the adsorption of NO_2 gas molecule on the defective Janus WSSe monolayer to be chemisorption. The physical-to-chemical adsorption transition caused by the introduction of Se vacancy allows Janus WSSe monolayers to satisfy the different demands of different gas sensitive installations. The physisorption of NO_2 gas molecule combined with the short recovery time makes the pristine Janus WSSe monolayer suitable for collecting and storing gases at low temperatures. Meanwhile, the powerful chemisorption of NO_2 gas molecule affords defective Janus WSSe monolayers the potential to activate and reduce NO_2 used for NO_2 gas conversion. Our studies opens a new path for the adsorption of NO_2 and provide a strong foundation for the development of the application of the Janus WSSe monolayer.

4. Computational Methods

In this study, the DFT calculations for the geometrical relaxation and electronic structure were carried out by using the Vienna Ab initio Simulation Package (VASP) (version 5.3, Hanger Group, University of Vienna) [49,50]. The generalized gradient approximation (GGA) method with Perdew–Burke–Ernzerhof (PBE) for the exchange–correlation energy was used. In order to describe the van der Waals (vdW) interaction between gas molecules and the substrate, we adopted the zero-damped DFT-D2 method proposed by Grimme [51]. The cutoff energy for the plane wave basis set was taken as 500 eV. During the optimization, all the internal coordinates were allowed to relax with a fixed lattice constant. Spin polarization was employed in the calculations of the adsorption of NO₂ since the molecule is paramagnetic [52]. A 4 × 4 supercell of pristine or defective WSSe monolayer, with a single gas molecule adsorbed on it, was chosen as the computational model. Brillouin zone was sampled for integration according to Monkhorst–Pack scheme [53] with a 2 × 2 × 1 K point sampling for thermodynamic stability and electronic properties calculations. A vacuum of 30 Å was provided along c-direction to avoid the effect of interlayer interaction. It has been shown that the DFT method is considered to be one of the most accurate methods for calculating the electronic structure of solids [54–56].

The adsorption energy (E_{ads}) of the NO₂ on the pristine and defective WSSe monolayer was calculated from [57,58] (Equation (1)),

$$E_{\text{ads}} = E_{\text{total}} - E_{\text{sub}} - E_{\text{gas}} \quad (1)$$

where E_{total} is the total energy of the gas-adsorbed monolayer, and E_{sub} and E_{gas} are the energies of the clean substrate (pristine or defective Janus WSSe monolayer) and the isolated NO₂ gas molecule, respectively. A negative value of E_{ads} indicates an exothermic adsorption. The more negative the E_{ads} is, the stronger the gas adsorption is.

The formation energy of defect x is defined by the following equation (Equation (2)),

$$E_{\text{vac}}^{\text{f}}(x) = E_{\text{def}}(x) - E_{\text{per}} - \mu_{\text{i}} \quad (2)$$

where $E_{\text{def}}(x)$ is the total energy of a system containing an x defect, E_{per} represents the energy of a perfect supercell, and μ_{i} is the energy of x atom. The value of μ_{i} largely depends on the experimental growth conditions. For the Janus WSSe monolayer, on the basis of the previous fabrication process [31,32], we considered the S-rich and Se-rich conditions as the limiting cases to discuss the $E_{\text{vac}}^{\text{f}}(x)$. In the thermodynamic equilibrium situation, one can assume that (Equation (3)),

$$\mu_{\text{wsse}} = \mu_{\text{w}} + \mu_{\text{s}} + \mu_{\text{se}} \quad (3)$$

where μ_{wsse} is the total energy per WSSe formula unit. Under the S-rich environment, the S chemical potential (μ_{s}^0) is equal to the total energy per S atom in the S₂ molecule. Then, the Se chemical potential can be written as (Equation (4)),

$$\mu_{\text{se(S-rich)}} = \mu_{\text{wsse}} - \mu_{\text{w}}^0 - \mu_{\text{s}}^0 \quad (4)$$

where μ_{w}^0 is the total energy per W atom in its stable bulk phase. Meanwhile, for the Se-rich condition, the Se chemical potential (μ_{se}^0) is equal to the total energy per Se atom in its reference phase, i.e., the Se bulk having body-centered-cubic structure. The S chemical potential can be written as (Equation (5)),

$$\mu_{\text{s(Se-rich)}} = \mu_{\text{wsse}} - \mu_{\text{w}}^0 - \mu_{\text{se}}^0 \quad (5)$$

The plane-integrated CDD was performed according to the following equation (Equation (6)),

$$\Delta\rho = \rho_{\text{total}} - \rho_{\text{sub}} - \rho_{\text{gas}} \quad (6)$$

where ρ_{total} , ρ_{sub} , and ρ_{gas} , respectively, are the charge density of the gas-adsorbed system, substrate, and NO_2 molecule.

From the Van't Hoff–Arrhenius theory, the recovery time, τ , can be estimated by [34,59] (Equation (7)):

$$\tau = \omega^{-1} \exp\left(\frac{E^*}{K_B T}\right) \quad (7)$$

where T , K_B , E^* , and ω stand for the temperature, Boltzmann Constant, desorption energy barrier, and attempt frequency, respectively. Here, E^* is approximated as the adsorption energy, while ω is assumed to be 10^{13} s^{-1} [34].

The strain is defined as (Equation (8))

$$\varepsilon = (a - a_0) / a_0 \quad (8)$$

where a_0 and a are the lattice parameters of the unit cell without and with strain, respectively. In this work, $-5\% \sim 5\%$ strain was considered, where the positive values mean tensile strains, while the negative values stand for compression strain.

The formation energy of the vacancy under the strain could be similarly defined by Equation (2), where $E_{\text{def}}(x)$ and E_{per} are the corresponding values under the same strain, respectively. μ_i , which is related only to the synthetic environment, has nothing to do with the exerted strain. Here, we define a new concept, E_{vac}^* , as follows (Equation (9)):

$$E_{\text{vac}}^*(x) = E_{\text{def}}(x) - E_{\text{per}} \quad (9)$$

Since the μ_i is constant with different strain, the effect of strain was identical for both $E_{\text{vac}}^*(x)$ and $E_{\text{vac}}^f(x)$. Therefore, in the following, we substituted E_{vac}^* for E_{vac}^f to study the strain effect for convenience. Moreover, the E_{vac}^* under no strain was chosen as a criterion. In this case, the positive relative E_{vac}^* implied the increase of the formation energy, and the negative relative E_{vac}^* indicated the decrease.

Supplementary Materials: The following supporting information can be downloaded at: <https://www.mdpi.com/article/10.3390/molecules28041644/s1>, Figure S1. The location of Se (a) and S vacancy defects (b) considered in our study; Figure S2. The relative E_{vac}^* of S vacancy under the different uniaxial (blue) and biaxial strains (orange); Table S1. The adsorption energy of NO_2 gas molecules on pristine and defective Janus WSSe monolayer; Table S2. The calculated charge of one Se atom from Janus WSSe monolayer under -10% , 0 and 10% strain.

Author Contributions: Supervision, L.J.; project administration, L.J. and H.Y.; Software, L.J. and X.L.; data curation, X.L. and X.Q.; formal analysis, B.L. and X.Q.; funding acquisition, L.J., Z.W. and H.Y.; investigation, Z.W., X.T., B.L. and L.J.; Writing—original draft, X.L., H.Y., X.T. and L.J. All authors have read and agreed to the published version of the manuscript.

Funding: This work is supported by Henan Scientific Research Fund for Returned Scholars, Open Project of Key Laboratory of Functional Materials and Devices for Informatics of Anhui Higher Education Institutes (Grant No. FSKFKT002), College Students Innovation Fund of Anyang Normal University (Grant No. 202210479049), National College Students Innovation and Entrepreneurship Training Program (Grant No. 202210479032), Henan College Key Research Project (Grant No. 22A140013), and Key Scientific Research Projects of the Higher Education Institutions of Henan Province (Grant No. 23A140015).

Institutional Review Board Statement: Not applicable.

Informed Consent Statement: Not applicable.

Data Availability Statement: The data presented in this study are available in Supplementary Materials.

Conflicts of Interest: The authors declare no conflict of interest.

References

1. Jorres, R.; Nowak, D.; Grimminger, F.; Seeger, W.; Oldigs, M.; Magnussen, H. The effect of 1 ppm nitrogen dioxide on bronchoalveolar lavage cells and inflammatory mediators in normal and asthmatic subjects. *Eur. Respir. J.* **1995**, *8*, 416–424. [[PubMed](#)]
2. Last, J.A.; Sun, W.-M.; Witschi, H. Ozone, NO, and NO₂: Oxidant air pollutants and more. *Environ. Health Persp.* **1994**, *102* (Suppl. S10), 179–184.
3. Zhai, L.; Zhang, J.; Wu, M.; Huo, H.; Bi, F.; Wang, B. Balancing good oxygen balance and high heat of formation by incorporating of -C(NO₂)₂F Moiety and Tetrazole into Furoxan block. *J. Mol. Struct.* **2020**, *1222*, 128934.
4. Krylov, I.B.; Budnikov, A.S.; Lopat'eva, E.R.; Nikishin, G.I.; Terent'ev, A.O. Mild Nitration of Pyrazolin-5-ones by a Combination of Fe(NO₃)₃ and NaNO₂: Discovery of a New Readily Available Class of Fungicides, 4-Nitropyrazolin-5-ones. *Chem. Eur. J.* **2019**, *25*, 5922–5933. [[CrossRef](#)] [[PubMed](#)]
5. Zhou, R.; Zhou, R.; Prasad, K.; Fang, Z.; Speight, R.; Bazaka, K.; Ostrikov, K. Cold atmospheric plasma activated water as a prospective disinfectant: The crucial role of peroxyxynitrite. *Green Chem.* **2018**, *20*, 5276–5284. [[CrossRef](#)]
6. Huang, L.; Wang, Z.; Zhang, J.; Pu, J.; Lin, Y.; Xu, S.; Shen, L.; Chen, Q.; Shi, W. Fully Printed, Rapid-Response Sensors Based on Chemically Modified Graphene for Detecting NO₂ at Room Temperature. *ACS Appl. Mater. Interfaces* **2014**, *6*, 7426–7433. [[CrossRef](#)]
7. Tang, H.; Lau, T.; Brassard, B.; Cool, W. A new all-season passive sampling system for monitoring NO₂ in air. *Field Anal. Chem. Technol.* **1999**, *3*, 338–345.
8. Palmes, E.D.; Gunnison, A.F.; DiMattio, J.; Tomczyk, C. Personal sampler for nitrogen dioxide. *Am. Ind. Hyg. Assoc. J.* **1976**, *37*, 570–577.
9. Colombo, M.; Nova, I.; Tronconi, E. Detailed kinetic modeling of the NH₃–NO/NO₂ SCR reactions over a commercial Cu-zeolite catalyst for Diesel exhausts after treatment. *Catal. Today* **2012**, *197*, 243–255.
10. Zhang, W.-J.; Bagreev, A.; Rasouli, F. Reaction of NO₂ with Activated Carbon at Ambient Temperature. *Ind. Eng. Chem. Res.* **2008**, *47*, 4358–4362.
11. Lee, G.; Yoo, D.K.; Ahmed, I.; Lee, H.J.; Jhung, S.H. Metal-organic frameworks composed of nitro groups: Preparation and applications in adsorption and catalysis. *Chem. Eng. J.* **2023**, *451*, 138538.
12. Baltrusaitis, J.; Jayaweera, P.M.; Grassian, V.H. XPS study of nitrogen dioxide adsorption on metal oxide particle surfaces under different environmental conditions. *Phys. Chem. Chem. Phys.* **2009**, *11*, 8295–8305. [[PubMed](#)]
13. Haubrich, J.; Quiller, R.G.; Benz, L.; Liu, Z.; Friend, C.M. In Situ Ambient Pressure Studies of the Chemistry of NO₂ and Water on Rutile TiO₂(110). *Langmuir* **2010**, *26*, 2445–2451.
14. Sivachandiran, L.; Thevenet, F.; Gravejat, P.; Rousseau, A. Investigation of NO and NO₂ adsorption mechanisms on TiO₂ at room temperature. *Appl. Catal. B-Environ.* **2013**, *142–143*, 196–204. [[CrossRef](#)]
15. Dalton, J.S.; Janes, P.A.; Jones, N.G.; Nicholson, J.A.; Hallam, K.R.; Allen, G.C. Photocatalytic oxidation of NO_x gases using TiO₂: A surface spectroscopic approach. *Environ. Pollut.* **2002**, *120*, 415–422. [[CrossRef](#)] [[PubMed](#)]
16. Epling, W.S.; Yezerets, A.; Currier, N.W. The effects of regeneration conditions on NO_x and NH₃ release from NO_x storage/reduction catalysts. *Appl. Catal. B-Environ.* **2007**, *74*, 117–129.
17. Choi, W.; Choudhary, N.; Han, G.H.; Park, J.; Akinwande, D.; Lee, Y.H. Recent development of two-dimensional transition metal dichalcogenides and their applications. *Mater. Today* **2017**, *20*, 116–130.
18. He, Q.; Zeng, Z.; Yin, Z.; Li, H.; Wu, S.; Huang, X.; Zhang, H. Fabrication of Flexible MoS₂ Thin-Film Transistor Arrays for Practical Gas-Sensing Applications. *Small* **2012**, *8*, 2994–2999.
19. Wehling, T.O.; Novoselov, K.S.; Morozov, S.V.; Vdovin, E.E.; Katsnelson, M.I.; Geim, A.K.; Lichtenstein, A.I. Molecular Doping of Graphene. *Nano Lett.* **2008**, *8*, 173–177. [[CrossRef](#)]
20. Schedin, F.; Geim, A.K.; Morozov, S.V.; Hill, E.W.; Blake, P.; Katsnelson, M.I.; Novoselov, K.S. Detection of individual gas molecules adsorbed on graphene. *Nat. Mater.* **2007**, *6*, 652–655.
21. Leenaerts, O.; Partoens, B.; Peeters, F.M. Adsorption of H₂O, NH₃, CO, NO₂, and NO on graphene: A first-principles study. *Phys. Rev. B* **2008**, *77*, 125416. [[CrossRef](#)]
22. Khan, A.F.; Brownson, D.A.C.; Randviir, E.P.; Smith, G.C.; Banks, C.E. 2D Hexagonal Boron Nitride (2D-hBN) Explored for the Electrochemical Sensing of Dopamine. *Anal. Chem.* **2016**, *88*, 9729–9737. [[CrossRef](#)]
23. Abbas, A.N.; Liu, B.; Chen, L.; Ma, Y.; Cong, S.; Aroonyadet, N.; Köpf, M.; Nilges, T.; Zhou, C. Black Phosphorus Gas Sensors. *ACS Nano* **2015**, *9*, 5618–5624. [[PubMed](#)]
24. Shukla, V.; Wärnå, J.; Jena, N.K.; Grigoriev, A.; Ahuja, R. Toward the Realization of 2D Borophene Based Gas Sensor. *J. Phys. Chem. C* **2017**, *121*, 26869–26876. [[CrossRef](#)]
25. Cui, S.; Pu, H.; Wells, S.A.; Wen, Z.; Mao, S.; Chang, J.; Hersam, M.C.; Chen, J. Ultrahigh sensitivity and layer-dependent sensing performance of phosphorene-based gas sensors. *Nat. Commun.* **2015**, *6*, 8632. [[PubMed](#)]
26. Ju, L.; Bie, M.; Tang, X.; Shang, J.; Kou, L. Janus WSSe Monolayer: An Excellent Photocatalyst for Overall Water Splitting. *ACS Appl. Mater. Interfaces* **2020**, *12*, 29335–29343. [[CrossRef](#)]
27. Ju, L.; Bie, M.; Zhang, X.; Chen, X.; Kou, L. Two-dimensional Janus van der Waals heterojunctions: A review of recent research progresses. *Front. Phys.* **2021**, *16*, 13201.
28. Ju, L.; Qin, J.; Shi, L.; Yang, G.; Zhang, J.; Sun, L. Rolling the WSSe Bilayer into Double-Walled Nanotube for the Enhanced Photocatalytic Water-Splitting Performance. *Nanomaterials* **2021**, *11*, 705.

29. Zhang, J.; Tang, X.; Chen, M.; Ma, D.; Ju, L. Tunable Photocatalytic Water Splitting Performance of Armchair MoSSe Nanotubes Realized by Polarization Engineering. *Inorg. Chem.* **2022**, *61*, 17353–17361. [[CrossRef](#)]
30. Yue, Q.; Shao, Z.; Chang, S.; Li, J. Adsorption of gas molecules on monolayer MoS₂ and effect of applied electric field. *Nanoscale Res. Lett.* **2013**, *8*, 425.
31. Lin, Y.C.; Liu, C.; Yu, Y.; Zarkadoula, E.; Yoon, M.; Puzos, A.A.; Liang, L.; Kong, X.; Gu, Y.; Strasser, A.; et al. Low Energy Implantation into Transition-Metal Dichalcogenide Monolayers to Form Janus Structures. *ACS Nano* **2020**, *14*, 3896–3906. [[PubMed](#)]
32. Zheng, B.; Ma, C.; Li, D.; Lan, J.; Zhang, Z.; Sun, X.; Zheng, W.; Yang, T.; Zhu, C.; Ouyang, G.; et al. Band Alignment Engineering in Two-Dimensional Lateral Heterostructures. *J. Am. Chem. Soc.* **2018**, *140*, 11193–11197. [[CrossRef](#)] [[PubMed](#)]
33. Cui, H.; Jiang, J.; Gao, C.; Dai, F.; An, J.; Wen, Z.; Liu, Y. DFT study of Cu-modified and Cu-embedded WSe₂ monolayers for cohesive adsorption of NO₂, SO₂, CO₂, and H₂S. *Appl. Surf. Sci.* **2022**, *583*, 152522.
34. Ma, D.; Ju, W.; Li, T.; Zhang, X.; He, C.; Ma, B.; Lu, Z.; Yang, Z. The adsorption of CO and NO on the MoS₂ monolayer doped with Au, Pt, Pd, or Ni: A first-principles study. *Appl. Surf. Sci.* **2016**, *383*, 98–105.
35. Chaurasiya, R.; Dixit, A.; Pandey, R. Strain-mediated stability and electronic properties of WS₂, Janus WSSe and WSe₂ monolayers. *Superlattices Microstruct.* **2018**, *122*, 268–279.
36. Jin, C.; Tang, X.; Tan, X.; Smith, S.C.; Dai, Y.; Kou, L. A Janus MoSSe monolayer: A superior and strain-sensitive gas sensing material. *J. Mater. Chem. A* **2019**, *7*, 1099–1106.
37. Ju, L.; Xu, T.; Zhang, Y.; Shi, C.; Sun, L. Ferromagnetism of Na_{0.5}Bi_{0.5}TiO₃ (1 0 0) surface with O₂ adsorption. *Appl. Surf. Sci.* **2017**, *412*, 77–84.
38. Ju, L.; Dai, Y.; Wei, W.; Li, M.; Huang, B. DFT investigation on two-dimensional GeS/WS₂ van der Waals heterostructure for direct Z-scheme photocatalytic overall water splitting. *Appl. Surf. Sci.* **2018**, *434*, 365–374. [[CrossRef](#)]
39. Ju, L.; Liu, C.; Shi, L.; Sun, L. The high-speed channel made of metal for interfacial charge transfer in Z-scheme g-C₃N₄/MoS₂ water-splitting photocatalyst. *Mater. Res. Express* **2019**, *6*, 115545. [[CrossRef](#)]
40. Wang, Y.; Chen, R.; Luo, X.; Liang, Q.; Wang, Y.; Xie, Q. First-Principles Calculations on Janus MoSSe/Graphene van der Waals Heterostructures: Implications for Electronic Devices. *ACS Appl. Nano Mater.* **2022**, *5*, 8371–8381.
41. Lee, G.-D.; Wang, C.Z.; Yoon, E.; Hwang, N.-M.; Kim, D.-Y.; Ho, K.M. Diffusion, Coalescence, and Reconstruction of Vacancy Defects in Graphene Layers. *Phys. Rev. Lett.* **2005**, *95*, 205501. [[CrossRef](#)] [[PubMed](#)]
42. Cho, B.; Hahm, M.G.; Choi, M.; Yoon, J.; Kim, A.R.; Lee, Y.-J.; Park, S.-G.; Kwon, J.-D.; Kim, C.S.; Song, M.; et al. Charge-transfer-based Gas Sensing Using Atomic-layer MoS₂. *Sci. Rep.* **2015**, *5*, 8052. [[PubMed](#)]
43. Kou, L.; Frauenheim, T.; Chen, C. Phosphorene as a Superior Gas Sensor: Selective Adsorption and Distinct I–V Response. *J. Phys. Chem. Lett.* **2014**, *5*, 2675–2681. [[CrossRef](#)] [[PubMed](#)]
44. Nolan, M.; Parker, S.C.; Watson, G.W. Reduction of NO₂ on Ceria Surfaces. *J. Phys. Chem. B* **2006**, *110*, 2256–2262. [[CrossRef](#)]
45. Zhao, S.; Tang, X.; Li, J.; Zhang, J.; Yuan, D.; Ma, D.; Ju, L. Improving the Energetic Stability and Electrocatalytic Performance of Au/WSSe Single-Atom Catalyst with Tensile Strain. *Nanomaterials* **2022**, *12*, 2793.
46. Hu, H.; Zhang, Z.; Ouyang, G. Transition from Schottky-to-Ohmic contacts in 1T VSe₂-based van der Waals heterojunctions: Stacking and strain effects. *Appl. Surf. Sci.* **2020**, *517*, 146168. [[CrossRef](#)]
47. Chen, D.; Lei, X.; Wang, Y.; Zhong, S.; Liu, G.; Xu, B.; Ouyang, C. Tunable electronic structures in BP/MoSSe van der Waals heterostructures by external electric field and strain. *Appl. Surf. Sci.* **2019**, *497*, 143809. [[CrossRef](#)]
48. Deng, S.; Li, L.; Rees, P. Graphene/MoXY Heterostructures Adjusted by Interlayer Distance, External Electric Field, and Strain for Tunable Devices. *ACS Appl. Nano Mater.* **2019**, *2*, 3977–3988.
49. Kohn, W.; Sham, L.J. Self-Consistent Equations Including Exchange and Correlation Effects. *Phys. Rev.* **1965**, *140*, A1133–A1138.
50. Hohenberg, P.; Kohn, W. Density functional theory (DFT). *Phys. Rev.* **1964**, *136*, B864. [[CrossRef](#)]
51. Grimme, S.; Antony, J.; Ehrlich, S.; Krieg, H. A consistent and accurate ab initio parametrization of density functional dispersion correction (DFT-D) for the 94 elements H–Pu. *J. Chem. Phys.* **2010**, *132*, 154104. [[CrossRef](#)] [[PubMed](#)]
52. Lunsford, J.H. EPR spectra of radicals formed when NO₂ is adsorbed on magnesium oxide. *J. Colloid Interf. Sci.* **1968**, *26*, 355–360. [[CrossRef](#)]
53. Monkhorst, H.J.; Pack, J.D. Special points for Brillouin-zone integrations. *Phys. Rev. B* **1976**, *13*, 5188. [[CrossRef](#)]
54. Hassan, A.; Ismail, M.; Reshak, A.H.; Zada, Z.; Khan, A.A.; Rehman, M.F.U.; Arif, M.; Siraj, K.; Zada, S.; Murtaza, G.; et al. Effect of heteroatoms on structural, electronic and spectroscopic properties of polyfuran, polythiophene and polypyrrole: A hybrid DFT approach. *J. Mol. Struct.* **2023**, *1274*, 134484.
55. Yu, H.; Huang, H.; Reshak, A.H.; Auluck, S.; Liu, L.; Ma, T.; Zhang, Y. Coupling ferroelectric polarization and anisotropic charge migration for enhanced CO₂ photoreduction. *Appl. Catal. B-Environ.* **2021**, *284*, 119709. [[CrossRef](#)]
56. Ullah, R.; Reshak, A.H.; Ali, M.A.; Khan, A.; Murtaza, G.; Al-Anazy, M.; Althib, H.; Flemban, T.H. Pressure-dependent elasto-mechanical stability and thermoelectric properties of MYbF₃ (M = Rb, Cs) materials for renewable energy. *Int. J. Energy Res.* **2021**, *45*, 8711–8723.
57. Li, D.-H.; Li, Q.-M.; Qi, S.-L.; Qin, H.-C.; Liang, X.-Q.; Li, L. Theoretical Study of Hydrogen Production from Ammonia Borane Catalyzed by Metal and Non-Metal Diatom-Doped Cobalt Phosphide. *Molecules* **2022**, *27*, 8206.

58. Liu, X.; Xu, Y.; Sheng, L. Al-Decorated C₂N Monolayer as a Potential Catalyst for NO Reduction with CO Molecules: A DFT Investigation. *Molecules* **2022**, *27*, 5790. [[CrossRef](#)]
59. Zhang, Y.-H.; Chen, Y.-B.; Zhou, K.-G.; Liu, C.-H.; Zeng, J.; Zhang, H.-L.; Peng, Y. Improving gas sensing properties of graphene by introducing dopants and defects: A first-principles study. *Nanotechnology* **2009**, *20*, 185504. [[CrossRef](#)]

Disclaimer/Publisher's Note: The statements, opinions and data contained in all publications are solely those of the individual author(s) and contributor(s) and not of MDPI and/or the editor(s). MDPI and/or the editor(s) disclaim responsibility for any injury to people or property resulting from any ideas, methods, instructions or products referred to in the content.